Electromagnetically Induced Transparency by NMR

by

HyungBin Son

Submitted to the Department of Physics
in partial fulfillment of the requirements for the degree of

Bachelor of Science in Physics

at the

MASSACHUSETTS INSTITUTE OF TECHNOLOGY

[June 2004]
May 2003

Author . . . .
Department of Physics
May 7, 2003

Certified by . . . .
Isaac L. Chuang
Associate Professor
Thesis Supervisor

Accepted by . . . .
Professor David Pritchard
Senior Thesis Coordinator, Department of Physics
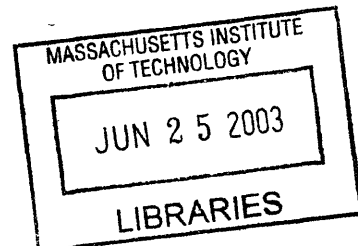
Electromagnetically Induced Transparency by NMR

by

HyungBin Son

Submitted to the Department of Physics
on May 8, 2003, in partial fulfillment of the
requirements for the degree of
Bachelor of Science in Physics

Abstract

Electromagnetically Induced Transparency (EIT) is a quantum nonlinear optical interference effect in which light at a certain frequency makes normally opaque atomic systems transparent to light at another frequency. Recent experiments in Atomic Molecular and Optical (AMO) physics demonstrated how the EIT effect can be used to store light pulses in an atomic system by coupling the light to the atomic system. One of the most elegant predictions of EIT theory is that the quantum phase of the dark state of the system remains unchanged even with a coupling between the dark state and another state. However, this has never been experimentally shown because of the lack of atomic systems that have long enough decoherence times and the difficulty of applying the complex pulse sequences needed to measure quantum phases in atomic systems. In this thesis, I use nuclear magnetic resonance techniques to implement the EIT effect and confirm this prediction, using Ramsey interferometry and visibility measurements to quantify the loss of quantum phase.

Thesis Supervisor: Isaac L. Chuang
Title: Associate Professor

Acknowledgments

Contents

Chapter 1

Introduction

1.1 Background

Electromagnetically Induced Transparency (EIT) is a quantum nonlinear optical interference effect in which a quantum system, that is normally opaque to light at a certain frequency, is made transparent in the presence of light at another frequency. Recent experiments in Atomic Molecular and Optical (AMO) physics have demonstrated how the EIT effect can be used to store pulses of light in an atomic system [HHDB99, LDBH01, PFWL01], which have been envisioned for applications in quantum information storage devices and long distance quantum communications. In this thesis, we explore the use of spin systems to implement the EIT effect using NMR.

1.2 Motivation

While the EIT effect is widely studied for important applications in quantum information processing [LYF00, DLCZ01] and the theories of the EIT effect is rather complete [HFK92, Har97, HH99, Pan01], it has not been extensively studied in nuclear spin systems. In particular, some of the theoretical predications have not been experimentally shown because of the lack of atomic systems that have long enough decoherence times and the lack of techniques to measure quantum phases in atomic systems. For example, in an EIT system, there exists a special state called "the dark state", in which the system is transparent to light at a certain frequency that it is normally opaque to. One of the most elegant predictions of EIT theory is that the quantum phase of the dark state remains unchanged. This has not

yet been shown due to the experimental difficulties with atomic systems mentioned above.

NMR techniques provide a good solution to observe this phenomenon due to the long decoherence times of nuclear spin systems and advanced techniques in manipulating nuclear spin systems. Moreover, there exist atom-like higher-order spin systems that can be used to effectively simulate atomic systems by NMR techniques [KF00, KSM+02]. In this thesis, we study how an higher-order spin system can be used to implement the EIT effect by NMR and confirm the transparency and the phase evolution of the dark state by Ramsey interferometry [SMP88].

1.3 Goals

The goal of this thesis is to implement the EIT effect using NMR quantum systems. More specifically, the goals are to

1. Introduce a higher-order spin system that is equivalent to an atomic system and show how a higher-order spin system can be used to efficiently simulate AMO physics. We then implement the EIT effect on this atom-like higher-order spin system using NMR techniques, characterize the transparency behavior of the system and provide experimental evidence of it.

2. Confirm that the quantum phase of the dark state remains unchanged by observing the Ramsey interference fringes through coupling to a reference state outside the EIT system. We also relate the transparency behavior to the visibility of the dark state.

1.4 Outline of the thesis

In chapter 2, we initiate our discussion by introducing the theory of the EIT effect and methods to characterize the transparency behavior. We also show that the EIT effect is an instance of quantum bang-bang control theory [VL98].

In chapter 3, we introduce a higher-order spin system and show its equivalence to a Λ-like atom cloud system. We then investigate two viable ways to prove the transparency behavior: observing the spin states of the system and measuring the visibility of the quantum states of the system through Ramsey interferometry. We also develop the analytic expressions for these measurable quantities.

In chapter 4, we present the experimental data and discuss the results. The experimental results are not only compared to the ideal results from the expressions developed in chapter 3, but also to our simulations which include the decoherence effects through the Lindblad formulation, the Bloch-Siegert shifts and the RF inhomogenity of the NMR probe. By comparing the experimental results to the theoretical predictions and our simulations, we conclude that the experimental results provide conclusive evidence that our spin system indeed becomes transparent to light and that the dark state in EIT does maintain phase coherence, as theoretically predicted.

Chapter 2

Theory of the EIT effect

Electromagnetically Induced Transparency (EIT) is a quantum nonlinear optical interference effect in which a quantum system, that is normally opaque to light at a certain frequency, is made transparent in the presence of light at another frequency. In this chapter, we introduce the well-known theory of the EIT effect in a three-level quantum system and study the ways to characterize the transparency behavior. We also present our new observation of the fact that the EIT effect is an instance of quantum bang-bang control theory.

2.1 Introduction to the EIT effect

Consider a Λ-like three-level atomic system (see Fig 2-1) and denote its energy eigenstates as $|1\rangle$, $|2\rangle$ and $|3\rangle$. The energy difference between the $|1\rangle$ and $|2\rangle$ states corresponds to ω_{probe} and between the $|2\rangle$ and $|3\rangle$ states corresponds to $\omega_{control}$. Suppose that two electromagnetic fields are applied simultaneously to the system: the probe field at frequency ω_{probe} with strength a and the control field at frequency $\omega_{control}$ with strength b.

Then the Hamiltonian describing the system (EIT Hamiltonian) is the following in the $|1\rangle$, $|2\rangle$ and $|3\rangle$ basis:

$$H_{EIT,a,b} = \begin{bmatrix} 0 & a^* & 0 \\ a & 0 & b^* \\ 0 & b & 0 \end{bmatrix} \tag{2.1}$$

The numbers a and b can in general be complex, but we assume them to be real here for simplicity. This is justified by the fact that, in practice, the NMR setup for our experiments is carefully calibrated so that these numbers are real.
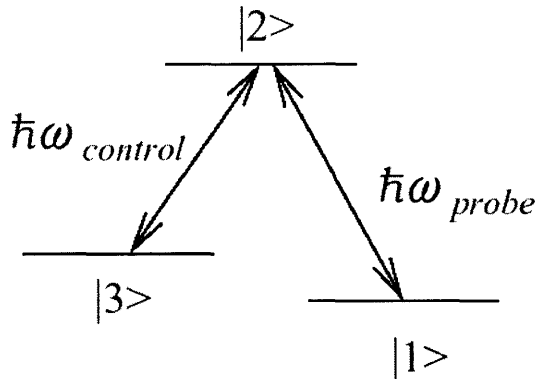
Figure 2-1: Energy level diagram of Λ-like atomic system.

2.2 The EIT effect in the presence of strong control field

The time evolution of the system while the EIT Hamiltonian is applied (EIT evolution) is given by

$$U_{EIT,a,b} = e^{-iH_{EIT,a,b}} \tag{2.2}$$

Solving for $U_{EIT,a,b}$, we obtain

$$U_{EIT,a,b} \approx \begin{bmatrix} 1 & i\frac{a}{b}\sin b & \frac{a}{b}(\cos b - 1) \\ i\frac{a}{b}\sin b & \cos b & i\sin b \\ \frac{a}{b}(\cos b - 1) & i\sin b & \cos b \end{bmatrix} \tag{2.3}$$

to the first order in $\frac{a}{b}$.

Suppose the system starts from the state $|1\rangle$. From Eq. (2.3), we observe that, in the limit $b \gg a$, all the terms connecting the state $|1\rangle$ and the rest of the states become zero. In other words, due to a quantum interference effect between the two interactions, the system does not absorb the photons at frequency ω_{probe} and thus the probe field does not have any effect on the system. As a result, the system becomes transparent to the electromagnetic radiation at frequency ω_{probe}.

We propose to measure this transparency behavior on a spin system in the next few sections. Before that we discuss our observation of EIT being an instance of quantum bang-bang control theory [VL98].

14

2.3 Quantum control

Consider the case when we have two Hamiltonians active on a system, with one being much higher in intensity than the other. The end-result of quantum-bang-bang control is that we can approximate the unitary evolution of the system as,

$$\sum_k^N U_k h U_k^\dagger = 0, \tag{2.4}$$

where h is the weak Hamiltonian, U_k are a set of unitary operators corresponding to the strong Hamiltonian, k is the index into the set and N is the size of the set.

In our case, h and U_k are given by,

$$h = h_a, \tag{2.5}$$

$$U_k = e^{i\frac{h_b}{N}k} \tag{2.6}$$

where h_a and h_b describe the interaction with the probe field and the control field, respectively:

$$h_a = \begin{bmatrix} 0 & a & 0 \\ a & 0 & 0 \\ 0 & 0 & 0 \end{bmatrix}, h_b = \begin{bmatrix} 0 & 0 & 0 \\ 0 & 0 & b \\ 0 & b & 0 \end{bmatrix}. \tag{2.7}$$

Here we prove that the quantum bang-bang control relation Eq. (2.4) holds in the presence of a strong control field and, thus, the interaction with the probe field diminishes. The time evolution of the system, in the limit $b \gg a$, is given by

$$\lim_{b \gg a} e^{-i(h_a + h_b)} \approx \prod_{k=0}^{N-1} e^{i\frac{h_a}{N}} e^{i\frac{h_b}{N}} \tag{2.8}$$

$$\approx \lim_{N \to \infty} \prod_{k=0}^{N-1} e^{-i\frac{h_a}{N}} e^{-i\frac{h_b}{N}} \tag{2.9}$$

$$= \lim_{N \to \infty} \left[\prod_{k=0}^{N-1} e^{-i\frac{k}{N}h_b} e^{-i\frac{h_a}{N}} e^{i\frac{k}{N}h_b} \right] e^{-ih_b}. \tag{2.10}$$

15

$$= \lim_{N\to\infty} \left[\prod_{k=0}^{N-1} U_k e^{-i\frac{h_a}{N}} U_k^\dagger \right] e^{-ih_b} \tag{2.11}$$

where $U_k = e^{-i\frac{k}{N}h_b}$, and

$$= \lim_{N\to\infty} \left[\prod_{k=0}^{N-1} e^{-iU_k \frac{h_a}{N} U_k^\dagger} \right] e^{-ih_b} \tag{2.12}$$

$$= \lim_{N\to\infty} e^{\left(\sum_{k=0}^{N-1} -\frac{i}{N} U_k h_a U_k^\dagger\right)} e^{(-ih_b)} \tag{2.13}$$

$$= e^{-iS} e^{-ih_b} \tag{2.14}$$

where,

$$S = \lim_{N\to\infty} \sum_{k=0}^{N-1} U_k \frac{h_a}{N} U_k^\dagger \tag{2.15}$$

which can be rewritten as

$$S = \lim_{N\to\infty} \sum_{k=0}^{N-1} \frac{1}{N} \begin{bmatrix} 0 & a\cos\frac{bk}{N} & ia\sin\frac{bk}{N} \\ a\cos\frac{bk}{N} & 0 & 0 \\ -ia\sin\frac{bk}{N} & 0 & 0 \end{bmatrix}$$

$$= \frac{1}{b} \int_0^1 \begin{bmatrix} 0 & a\cos x & ia\sin x \\ a\cos x & 0 & 0 \\ -ia\sin x & 0 & 0 \end{bmatrix} dx \tag{2.16}$$

where $x = bk/N$,

$$= \begin{bmatrix} 0 & \frac{a}{b}\sin b & -i\frac{a}{b}(\cos b - 1) \\ \frac{a}{b}\sin b & 0 & 0 \\ i\frac{a}{b}(\cos b - 1) & 0 & 0 \end{bmatrix} \tag{2.17}$$

Thus, in the limit $b \gg a$, the Hamiltonian $S \to 0$. We then have from Eq. (2.8)-(2.14),

16

$$\lim_{b \gg a} e^{-i(h_a + h_b)} \approx \lim_{b \gg a} e^{-iS} e^{-ih_b} = e^{-ih_b} = \begin{bmatrix} 1 & 0 & 0 \\ 0 & \cos b & i \sin b \\ 0 & i \sin b & \cos b \end{bmatrix} \qquad (2.18)$$

The terms related to the interaction with the probe field are eliminated due to the quantum control and only the terms related to the control field are present. Note the result is the same as Eq. (2.3) in the limit $b \gg a$.

2.4 Dark state

In this section, we discuss the case of the EIT effect with an interesting quantum state called the dark state. Suppose the system is in the eigenstate of $H_{EIT,a,b}$ with eigenvalue zero. Now the applied fields do not change the state of the system. As the applied fields do not interact with the system, the system becomes transparent to the incident fields and this eigenstate of $H_{EIT,a,b}$ is called the dark state. The eigenvector matrix of $H_{EIT,a,b}$ is

$$V = \sqrt{\frac{b^2}{2(a^2 + b^2)}} \begin{bmatrix} a/b & a/b & -\sqrt{2} \\ \sqrt{b^2 + a^2}/b & -\sqrt{b^2 + a^2}/b & 0 \\ 1 & 1 & \sqrt{2}a/b \end{bmatrix} \qquad (2.19)$$

where the eigenvectors are given as column vectors of V. Only the third eigenvector has an eigenvalue of zero and thus represents the dark state of the three level system. Denote the dark state as $|D_{a,b}\rangle$.

$$|D_{a,b}\rangle = \sqrt{\frac{b^2}{a^2 + b^2}} \begin{pmatrix} 1 \\ 0 \\ -a/b \end{pmatrix} \qquad (2.20)$$

The dark state does not change over the EIT evolution

$$U_{EIT,a,b}|D_{a,b}\rangle = |D_{a,b}\rangle \qquad (2.21)$$

as $H_{EIT,a,b}|D_{a,b}\rangle = 0$.

$|D_{a,b}\rangle$ approaches the state $|1\rangle$ in the $b \gg a$ limit, the condition in which most EIT experiments have been carried out.

In this thesis, the dark state is investigated in two cases: $a = b$ and $b \gg a$. From here on, we call this dark state in the $b \gg a$ limit, i.e. $|1\rangle$, "the dark state" without any further description and the dark state at a specific ratio of the probe field strength α and the control field strength β as $|D_{\alpha,\beta}\rangle$.

Chapter 3

Methods to verify the transparency behavior by NMR

Generally, the transparency behavior of an EIT system is verified by directly measuring the output light intensity of the probe field passing through the system. However, this is not possible with NMR quantum systems. In this chapter, we first introduce the equivalence of a higher-order spin system to a Λ-like atomic system. Then we investigate the transparency behavior of our system more rigorously. We relate the evolution of the state of the system with the amount of photon absorbtion and define the transparency value of our system. Finally, we present two ways of verifying the transparency behavior of our system. The first one is observing the NMR signal corresponding to obserables of the density matrix of the system. This serves as the first check to ensure the transparency behavior in the $b \gg a$ limit. The other is measuring the visibility of the dark state after the EIT evolution. Finally, we also show the phase coherence of the system through Ramsey interferometry.

3.1   Higher-order spin system

In this section, we briefly introduce a higher-order spin system to help us to understand its equivalence to an atomic system. However, the experimental details are given in chapter 4.

The system we use to demonstrate the EIT effect is the spin-7/2 ^{133}Cs nucleus of a molecule in liquid crystal phase (see Fig. 3-1). The transition frequencies are split due to a quadrupole interaction between the nucleus and the liquid crystal environment.

19

The Hamiltonian for a quadrupolar system [Abr83, Sli96] can be written as:

$$\mathcal{H}_0 = -\hbar\omega_0 I_z \frac{e^2 qQ}{4I(2I-1)}(3I_z^2 - I(I+1)) \tag{3.1}$$

where eq is the electric field gradient, eQ the quadrupole moment, I_z is the $\hat{z}$ angular moment operator, and I is the spin of the nucleus.

The Hamiltonian has $2I + 1$ energy eigenstates labeled by I_z. Thus the spin-7/2 ^{133}Cs nucleus has eight energy levels. For our experiments, only the subsystem of spin $I_z = $ -3/2, -1/2, 1/2, 3/2 states are used, thus we consider only these states for our discussion.

The states $|1\rangle$, $|2\rangle$ and $|3\rangle$ are used for the EIT evolution (compare Fig. 2-1 and Fig. 3-1). The state $|R\rangle$ is used as the "reference state", whose use is made clear in the subsequent sections.

$$I_z$$
(Spin Angular Momentum)

$-3/2$ ————————↑——————————— $|R\rangle$

$\hbar\omega_R$

$-1/2$ ————————↓↑——————————— $|1\rangle$

$\hbar\omega_{probe}$

$1/2$ ————————↓↑——————————— $|2\rangle$

$\hbar\omega_{control}$

$3/2$ ————————↓——————————— $|3\rangle$
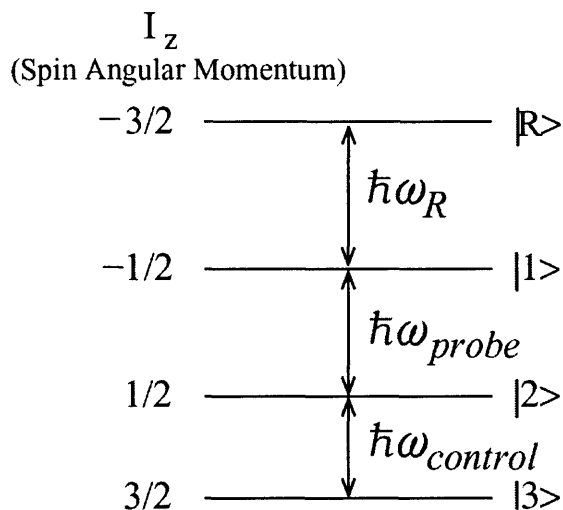
Figure 3-1: Schematic energy level diagram for the $I_z = -3/2, -1/2, 1/2, 3/2$ subsystem of $I = 7/2$ system with quadrupole splitting.

3.2 State evolution and a measure of transparency

We first start by understanding the transparency in the simplest possible system: a two-level system. Consider a two-level system whose transition frequency is ω (see Fig. 3-2).

The Hamiltonian describing this system is

$$H = \begin{bmatrix} 0 & 0 \\ 0 & \hbar\omega \end{bmatrix} \quad (3.2)$$

in the $|1\rangle$, $|2\rangle$ basis.
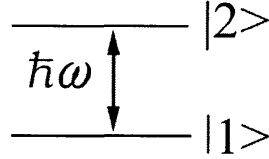
Figure 3-2: A two state system with transition frequency ω.

Suppose that the only interaction allowed in the system is the interaction with the photons at frequency ω and the rate of the spontaneous emission of the photons is negligible compared to the strength of the interaction. The system starts from the state $|1\rangle$, interacts with the electromagnetic field at at frequency ω and ends at a state $|\phi_{final,a,b}\rangle$. When we have a large ensemble of such systems, according to the energy conservation principle, the difference of the expected energy of the state $|\phi_{final,a,b}\rangle$ and the state $|1\rangle$ is proportional to the net number of photons absorbed at frequency ω.

$$\Delta E = \langle\phi_{final,a,b}|H|\phi_{final,a,b}\rangle - \langle 1|H|1\rangle = \hbar\omega|\langle 2|\phi_{final,a,b}\rangle|^2 = \hbar\omega(1-|\langle 1|\phi_{final,a,b}\rangle|^2) \quad (3.3)$$

We define the transparency value as the following:

$$T = \frac{\Delta E}{\hbar\omega} - 1 = |\langle 1|\phi_{final,a,b}\rangle|^2 = |\langle 1|U_{field}|1\rangle|^2 \quad (3.4)$$

where U_{field} is the system evolution due to the interaction between the electromagnetic field and the system. The transparency value equals to the square expectation of the state $|1\rangle$ over the system evolution.

The transparency value is one when the system has not aborbed any photons or the number of photons absorbed is the same as the number of photons emitted and zero when the system has absorbed photons to its maximum capacity. Thus $1 - T$ is proportional to the net number of photons absorbed.

Now, let's return to our system (see Fig. 2-1 and 3-1). Ignore the presence of the state $|R\rangle$ for now. The difference between our system and the two-level example discussed is that we have one additional state labeled as $|3\rangle$. Suppose the system also starts from the state $|1\rangle$, interacts with the electromagnetic radiation at frequency ω_{probe} and ends at the state $|\phi_{final,a,b}\rangle$. The transparency value in this case is given as:

$$T = |\langle 1|\phi_{final,a,b}\rangle|^2 = |\langle 1|U|1\rangle|^2 = 1 - |\langle 2|\phi_{final,a,b}\rangle|^2 - |\langle 3|\phi_{final,a,b}\rangle|^2 \qquad (3.5)$$

This value tells us how much of the population still remains in the state $|1\rangle$, hence an indicator of transparency.

3.3 Density matrix in the strong control field limit

In this section, we carefully look into the quantum state evolution when the system starts from the state $|1\rangle$ and discuss the relation between the density matrix and the transparency behavior of the system in the $b \gg a$ limit. Suppose the system starts from the state $|1\rangle$

$$|\phi_0\rangle = \begin{pmatrix} 1 \\ 0 \\ 0 \end{pmatrix} \qquad (3.6)$$

Then the final state of the system is given by

$$|\phi_{final,a,b}\rangle = U_{EIT,a,b}|\phi_0\rangle = \begin{pmatrix} \frac{b^2}{l^2} + \frac{a^2}{l^2}\cos l \\ -i\frac{a}{l}\sin l \\ \frac{ab}{l^2}(\cos l - 1) \end{pmatrix} \approx \begin{pmatrix} 1 \\ -i\frac{a}{b}\sin b \\ \frac{a}{b}(\cos b - 1) \end{pmatrix} \qquad (3.7)$$

to the first order in $\frac{a}{b}$, where $l = \sqrt{a^2 + b^2}$. The transparency value can be calculated from $|\langle 1|\phi_{final,a,b}\rangle|$ or $|\langle 2|\phi_{final,a,b}\rangle|$ and $|\langle 3|\phi_{final,a,b}\rangle|$. These quantities, however, are not directly observable in NMR experiments. We inquire into the observables of the system and find that $|\langle 2|\phi_{final,a,b}\rangle|$ can be estimated from the $|2\rangle\langle 1|$ component of the density matrix:

$$\langle 2|\phi_{final,a,b}\rangle = \langle 2|\phi_{final,a,b}\rangle\langle \phi_{final,a,b}|\phi_{final,a,b}\rangle = \langle 2|\rho_{final}|\phi_{final,a,b}\rangle \approx \langle 2|\rho_{final}|1\rangle \quad (3.8)$$

22

where ρ_{final} is the density matrix after the EIT evolution

$$\rho_{final} = |\phi_{final,a,b}\rangle\langle\phi_{final,a,b}| \approx \begin{bmatrix} 1 & i\frac{a}{b}\sin b & \frac{a}{b}(\cos b - 1) \\ -i\frac{a}{b}\sin b & \frac{a^2}{b^2}\sin b^2 & -i\frac{a^2}{b^2}\sin b(\cos b - 1) \\ \frac{a}{b}(\cos b - 1) & i\frac{a^2}{b^2}\sin b(\cos b - 1) & \frac{a^2}{b^2}(\cos b - 1)^2 \end{bmatrix}$$

$$(3.9)$$

to the first order in a/b.

As the first check to the transparency behavior of our system in this limit, we measure the $|2\rangle\langle1|$ component of the density matrix. According to this theory, we expect it to exhibit Rabi oscillations with a decreasing amplitude of $\frac{a}{b}$ as $b \to \infty$, showing that the transparency value behaves like $1 - \frac{a^2}{b^2}$ as $b \to \infty$, which is consistent with Eq. 3.5 and 3.7:

$$T = |\langle 1|\phi_{final,a,b}\rangle|^2 = \frac{b^2 + a^2\cos l}{l^2} \approx 1 - \frac{a^2}{b^2}\cos l \tag{3.10}$$

This oscillatory behavior of the $|2\rangle\langle1|$ component with b also tells a important nature of the EIT evolution. The system alternates between absorbing and emitting photons at frequency ω_{probe} during the evolution. The transparency value is proportional to the net number of photons absorbed.

3.4 Visibility

In this section, we introduce the concept of visibility through a classical interference experiment and develop the notion of quantum visibility. We then relate this quantity to the transparency value. We also derive analytic expressions for the visibility of the dark state $|D_{\alpha,\beta}\rangle$.

3.4.1 Classical visibility of electromagnetic waves

Consider a two slit interference experiment (see Fig. 3-3). The incoming wave is a electromagnetic wave at frequency ω. A system that causes a signal amplitude decay of c and phase delay of ϕ to the wave passing through it is placed in front of one of the slits. As a result of interference, an intensity pattern $I(x)$ appears at position x on the screen. Suppose θ is the phase difference corresponding to the path difference. The intensity pattern is given by

$$I(\theta) = |1 + e^{i(\theta+\phi)}c|^2 = 1 + c^2 + 2c\cos(\theta + \phi) \tag{3.11}$$
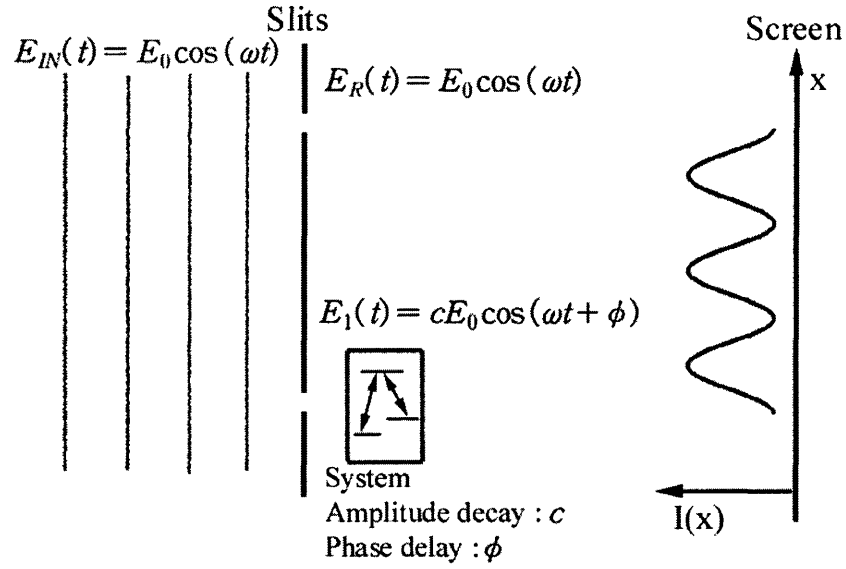
Figure 3-3: Two slit visibility experiment.

and the visibility is given by

$$V = \frac{I_{max} - I_{min}}{I_{max} + I_{min}} = \frac{2c}{1 + c^2} \qquad (3.12)$$

where $I_{max} = \max(I(\theta)) = (1 + c)^2$ and $I_{min} = \min(I(\theta)) = (1 - c)^2$. Thus, measuring the visibility gives the signal amplitude decay c and measuring the values of θ where I_{max} and I_{min} occur gives the phase shift ϕ.
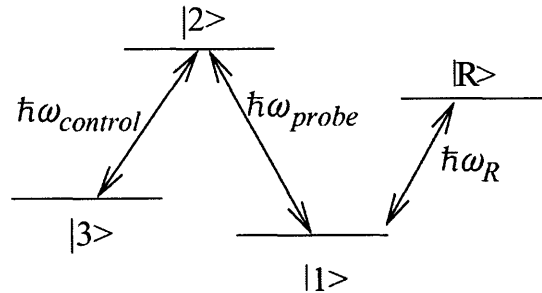
Figure 3-4: Energy level diagram of a Λ-like atomic system. $|R\rangle$ is a reference to measure the quantum phase of $|1\rangle$.
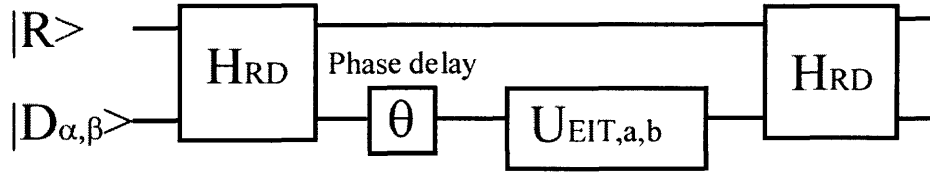
Figure 3-5: Quantum visibility experiment.

3.4.2 Quantum visibility

Suppose we have another state accessible: the state $|R\rangle$ (see Fig. 3-4). We can use this as a reference to measure the phase and the visibility of the dark state (see Fig. 3-5). Suppose the system starts in the state $|R\rangle$. Before applying the EIT Hamiltonian, we create an equal superposition of the $|R\rangle$ state and $|D_{\alpha,\beta}\rangle$ state to obtain $\frac{e^{i\theta}|D_{\alpha,\beta}\rangle+|R\rangle}{\sqrt{2}}$. This is done by applying a Hadamard gate in the the $|R\rangle$ and $|D_{\alpha,\beta}\rangle$ basis, followed by a $\hat{z}$-rotation to add an overall phase θ to the $|D_{\alpha,\beta}\rangle$ state. Then we apply an EIT evolution $U_{EIT,a,b}$, fixing the probe field strength a and varying the control field strength b. Finally, we again apply the Hadamard gate to obtain the expectation of the state $|R\rangle$.

This process is described by the following evolution matrix:

$$U = H_{RD}U_{EIT,a,b}e^{i\theta\sigma_z}H_{RD} \tag{3.13}$$

where H_{RD} is the Hadamard gate and σ_z is the Pauli sigma operator in the $|R\rangle$ and $|D_{\alpha,\beta}\rangle$ basis:

$$H_{RD} = \frac{1}{\sqrt{2}}\begin{bmatrix} 1 & 1 \\ 1 & -1 \end{bmatrix}, \tag{3.14}$$

$$\sigma_z = \frac{1}{2}\begin{bmatrix} 1 & 0 \\ 0 & -1 \end{bmatrix} \tag{3.15}$$

The final state of the system is

$$|\phi_{final,a,b}\rangle = U|R\rangle \tag{3.16}$$

and the expectation of the $|R\rangle$ is given by

$$|\langle R|\phi_{final,a,b}\rangle| = |\langle R|U|R\rangle| \tag{3.17}$$

25

Suppose $|D_{\alpha,\beta}\rangle$ is the dark state of the EIT Hamiltonian applied, i.e. $\beta/\alpha = b/a$. By the definition of the dark state, $U_{EIT,a,b}|D_{\alpha,\beta}\rangle = |D_{\alpha,\beta}\rangle$. Thus,

$$\langle R|U|R\rangle = \langle R|H_{RD}U_{EIT,a,b}e^{i\theta\sigma_z}H_{RD}|R\rangle = \langle R|H_{RD}e^{i\theta\sigma_z}H_{RD}|R\rangle = \cos(\theta/2) \qquad (3.18)$$

The intensity of the expectation of the state $|R\rangle$ is given by

$$I(\theta) = |\langle R|U|R\rangle|^2 = \frac{1 + p^2 + 2p\cos\theta}{4} \qquad (3.19)$$

where p is the expectation of the state $|R\rangle$ over the EIT evolution: $p \equiv \langle D_{a^*,b^*}|U_{EIT,a,b}|D_{\alpha,\beta}\rangle$. Note that $|\langle R|U|R\rangle|^2$ reduces to $\cos^2(\theta/2)$ when $p = 1$, which is the condition for the maximum visibility. We expect to see the Ramsey oscillations in the intensity.

The quantum visibility is defined in the same manner as the classical visibility in Eq. 3.12.

$$V = \frac{I_{max} - I_{min}}{I_{max} + I_{min}} = \frac{2p}{1 + p^2} \qquad (3.20)$$

The visibility is expected to approach one as p approaches one.
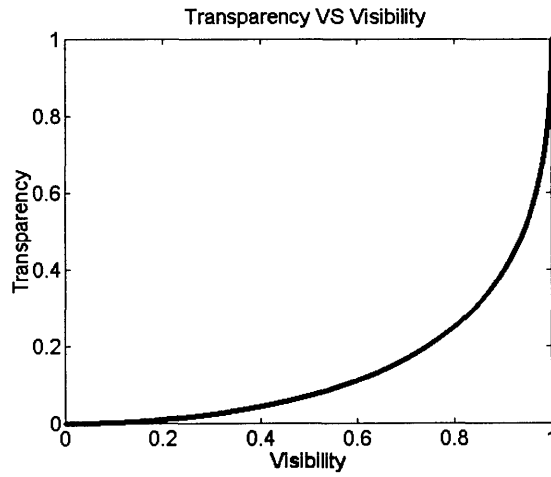
Figure 3-6: Transparency value versus visibility

From the expression for the visibility and for the transparency in terms of the expectation of the dark state over the EIT evolution (see Eq. (3.20) and (3.5)), the visibility and the transparency value can be related (see Fig. 3-6). The relation is a monotonically increasing one to one mapping ranging from zero to one:

$$V = \frac{2p}{1+p^2} = \frac{2\sqrt{T}}{1+T} \tag{3.21}$$

3.4.3 Visibility at specific ratios of β and α.

In this section, we derive the analytic expressions for the visibility at specific ratios of β and α.

When $\beta = \alpha$, the dark state $|D_{1,1}\rangle$ is the state $\frac{|1\rangle - |3\rangle}{\sqrt{2}}$ and the the expectation of the state $|D_{1,1}\rangle$ over the EIT evolution is

$$p = |\langle D_{1,1}|U_{EIT,a,b}|D_{1,1}\rangle| = \frac{(a+b)^2 + (a-b)^2 \cos l}{2l^2} \tag{3.22}$$

and the visibility is given by

$$V = \frac{2p}{1+p^2} = \frac{\frac{(a+b)^2 + (a-b)^2 \cos l}{l^2}}{1 + \left[\frac{(a+b)^2 + (a-b)^2 \cos l}{2l^2}\right]^2} \tag{3.23}$$

In the $\beta \gg \alpha$ limit, the dark state $|D_{\alpha,\beta}\rangle$ is the state $|1\rangle$ and the expectation of the state $|1\rangle$ over the EIT evolution is given in Eq 3.7:

$$p = \frac{b^2}{l^2} + \frac{a^2}{l^2} \cos l \tag{3.24}$$

and the visibility is given by

$$V = \frac{2p}{1+p^2} = \frac{2\left[\frac{b^2}{l^2} + \frac{a^2}{l^2} \cos l\right]}{1 + \left[\frac{b^2}{l^2} + \frac{a^2}{l^2} \cos l\right]^2} \tag{3.25}$$

With these analytic expressions in hand, we now test the transparency behavior of the spin system in the next chapter.

Chapter 4

Experimental realization of the EIT effect by NMR

In this chapter, we present the experimental data and discuss the results. The experimental results are not only compared to the ideal results from the expressions developed in chapter 3, but also to our simulations which include the decoherence effects through the Lindblad formulation, the Bloch-Siegert shifts and the RF inhomogenity of the NMR probe. By comparing the experimental results to the theoretical predictions and our simulations, we conclude that the experimental results provide conclusive evidence that our spin system indeed becomes transparent to light and that the dark state in EIT does maintain phase coherence, as theoretically predicted.

4.1   Experimental setup

All the experiments have been carried out using a Varian Unity Inova 11.7 Tesla 500 MHz NMR Spectrometer with a Varian H-X probe at Prof. Chuang's group. The system is the spin-7/2 ^{133}Cs nucleus of a pentadecauorooctanoate molecule in liquid crystal phase (see Fig. 3-1). ^{133}Cs nucleus has a Larmor frequency of 64.34 MHz at the given field strength. The transition frequencies are split due to a quadrupole interaction between the electric field gradient of the liquid crystal and the quadrupole moment of the ^{133}Cs nucleus. The temperature of the sample is set at $27°C$ to have an optimal balance between large quadrupole splittings and narrow linewidths. The three states with the largest decoherence times, the spin $I_z = $ -1/2, 1/2, 3/2 states, are used for EIT (see Fig. 2-1).

Highly selective Gaussian RF pulses with frequencies corresponding to $I_z = -1/2 \rightarrow$ 1/2 transition and $I_z = 1/2 \rightarrow 3/2$ transition are used as the probe field and control field, respectively. The length of the Gaussian pulses is $6ms$ for the EIT Hamiltonian and $620\mu s$ for the rest of the operations. The lengths of pulses are carefully selected so that the pulses are selective enough not to excite neighboring transitions yet the total experiment time is minimized. The EIT pulses are applied for a duration of $6ms$ to be able to sweep through a wide range of the control field. The transition frequencies are split by 7.5KHz and the line-widths for the transitions at ω_{probe} and $\omega_{control}$ are 2-3 Hz and 10-12Hz, respectively. The $T_1 \approx T_2$ relaxation time constants for the same transitions are about 55ms and 110ms, respectively.

In the high temperature approximation, the populations of the spin states are linear with the energy of the states [Fun01]. Thus it is impossible to start the system from a pure state such as the state $|1\rangle$. We resolve this problem by creating an "effective pure state" [GC97, CFH97]. This can be done by performing two experiments: **1.** with the thermal population distribution and **2.** with the populations of the state $|1\rangle$ and $|3\rangle$ interchanged.

$$\rho_1 = \begin{bmatrix} -3 & 0 & 0 & 0 \\ 0 & -1 & 0 & 0 \\ 0 & 0 & 1 & 0 \\ 0 & 0 & 0 & 3 \end{bmatrix}, \rho_2 = \begin{bmatrix} -3 & 0 & 0 & 0 \\ 0 & 3 & 0 & 0 \\ 0 & 0 & 1 & 0 \\ 0 & 0 & 0 & -1 \end{bmatrix} \quad (4.1)$$

$$\rho_{effective} = \rho_1 + \rho_2 = c_1 \begin{bmatrix} 1 & 0 & 0 & 0 \\ 0 & 0 & 0 & 0 \\ 0 & 0 & 0 & 0 \\ 0 & 0 & 0 & 0 \end{bmatrix} + c_2 I \quad (4.2)$$

where c_1 and c_2 are constants. $\rho_{effective}$ behaves like the pure state because the identity part of the density matrix does not evolve under unitary transformations and is not measurable in NMR. This technique is called the "temporal labeling" [KCL98].

The transparency behaviour is verified by observing the spin states. This is made possible by observing the NMR spectrum of the spins, which is the Fourier transform of the free induction decay (FID) signal. The time varying complex-valued voltage $V(t)$ measured by a pick-up coil around the sample,

$$V(t) = Tr\left[e^{-iHt}R\rho R^{\dagger}e^{iHt}\hat{O}\right]e^{-t/T_2}, \tag{4.3}$$

where, $\hat{O}$ is the measurement observable, $\hat{O} = \sum_{k=1,2}(\sigma_x^k - i\sigma_y^k)/2 = |R\rangle\langle 1| + |1\rangle\langle 2| + |2\rangle\langle 3|$ and T_2 is the transverse (phase) relaxtion time constant. The Fourier transform of the FID signal at frequency ω_{mix}, ω_{probe} and $\omega_{control}$ are proportional to the $|R\rangle\langle 1|$, $|1\rangle$ $\langle 2|$ and $|2\rangle$ $\langle 3|$ components of the density matrix, respectively.

4.2 Density matrix evolution in the strong control field limit

(a)   (b)
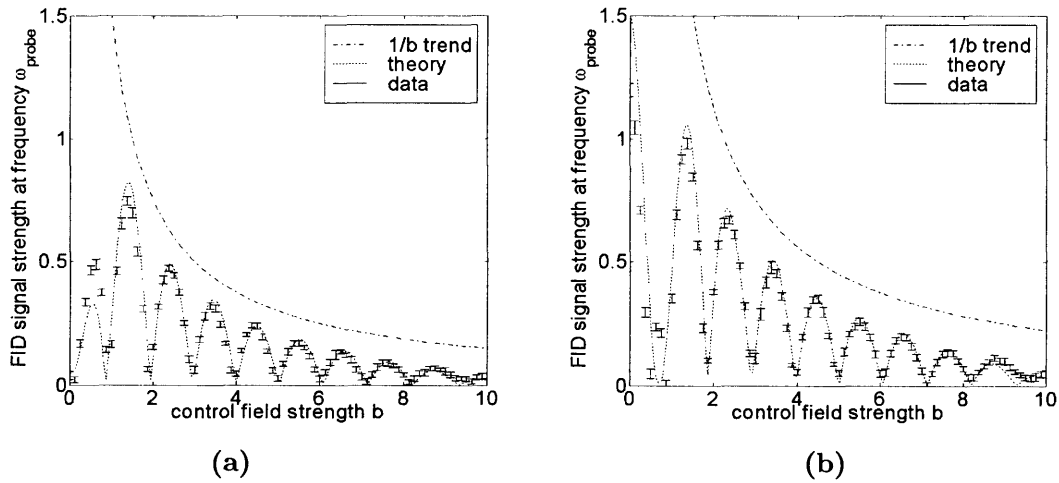
Figure 4-1: Fourier transformed free induction decay of V(t) when the the probe field strength corresponds to (a). π, (b). $3\pi/2$ pulses, respectively.

The experiments were performed at different fixed probe field strengths corresponding to π and $3\pi/2$ pulses, while varying the control field from 0 to a strength equivalent to 10π pulses (see section 3.3). The pulse sequence is given in Appendix D. The FID signal corresponding to the $|2\rangle\langle 1|$ component of the density matrix, with the EIT Hamiltonian turned on (see Eq. (3.9)), are normalized with respect to the readout of the thermal state and plotted in Fig. 4-1. Rabi oscillations of the $|2\rangle\langle 1|$ component of the density matrix with amplitude a/b are clearly seen. In fact, the amplitude decays faster than a/b, which we believe to be due to the RF inhomogenity of the NMR probe. The experimental results are compared to the simulation, which includes the effects of the Bloch-Siegert shift and the RF inhomogenity (see Appendix A). The Bloch-Siegert is a phenomenon wherein an off-resonance excitation far from the resonance frequency induces $\hat{z}$-rotations on a quantum

state [SVC00]. Our result confirms the transparency behavior of the system in the strong control field limit (see section 3.3).

4.3 Ramsey oscillations with coherent dark state

Ramsey interferometry with the states $|D_{1,1}\rangle$ and $|R\rangle$ is carried out (see section 3.4.2). Both the probe field and the control field strength is set to a $\pi/2$ pulse. The detailed pulse sequence is given in Appendix E.
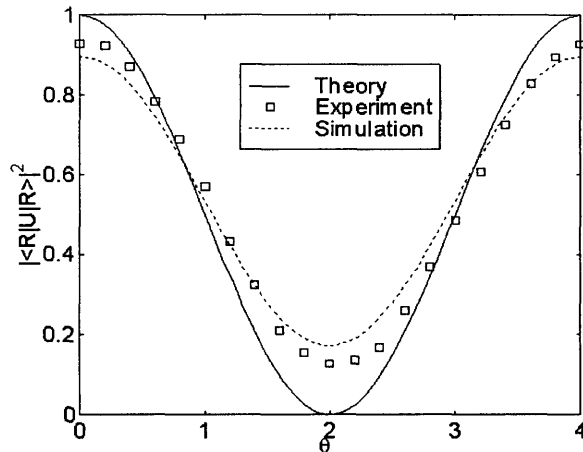
Figure 4-2: The square expectation of the reference state $|R\rangle$ as a function of θ. The horizontal axis is the phase shift introduced θ in units of $\pi/2$. The solid line is the expected $\cos^2(\theta/2)$ behavior (see Eq. (3.18)). The squares are the experimental results and the experimental random errors are smaller than the size of the squares. The dotted line is the simulation, which includes the decoherence effects. The minimum occurs at $\theta = \pi$ and the maximum occurs at $\theta = 0$, which is consistent with the prediction of the quantum phase of the dark state due to the EIT evolution.

The intensity in the expectation of the reference state $|R\rangle$ is plotted as a function of θ, the phase between the state $|D_{1,1}\rangle$ and $|R\rangle$ (see Fig. 4-2). The intensity exhibits the expected $\cos^2(\theta/2)$ behavior (see Eq. (3.18)). The minimum occurs at $\theta = \pi$ and the maximum occurs at $\theta = 0$, which is consistent with the prediction of the quantum phase of the dark state due to the EIT evolution.

The experimental errors are obtained by repeating the experiment three times and taking the random errors and are smaller than the size of the squares. We believe that the sources of the errors are the noise in the FID signal and the temperature fluctuations in the experimental setup. Because the electric field gradient of the liquid crystal is extremely sen-

sitive to the temperature, the resonance frequencies of individual transitions are extremely sensitive to it, too. We have experienced that $1°C$ deviation in the temperature can change the resonance frequencies by about 400Hz in the experiments.

The simulation includes decoherence effects, which are significant because the duration of the experiments, which is about $12.4ms$, is about 1/4 of the relaxation times of the system. The decoherence effects are modeled using the Lindblad formulation for higher-order spins [Mur03] (see Appendix C).

In the following section, we carry out the same experiment while varying varying the control field strength and study how the visibility of the state $|R\rangle$ behaves.

4.4 Visibility with coherent dark state

Ramsey interferometry with the states $|D_{1,1}\rangle$ and $|R\rangle$ is carried out. The probe field strength a is set to a power corresponding to a $\pi/2$ pulse and the control field strength is varied from $\pi/2$ to 5π pulses. The detailed pulse sequence is given in Appendix E.
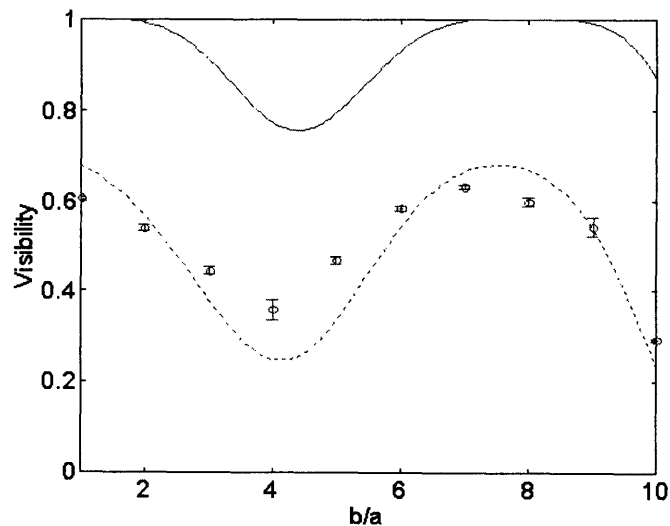
Figure 4-3: Visibility when $\beta/\alpha = 1$. Due to the decoherence effects, the experimental results (bars) falls far below the theory (solid line). The simulation (dotted line) includes the decoherence effects and the imperfectness of the probe field and the control field strengths

We plot the visibility of the state $|R\rangle$ in Fig. 4-3. The solid line is the theoretical result (see Eq. (3.23)), the error bars are the data and the dotted line is the simulation. In addition to decoherence effects, the simulation includes the imperfections of the probe and

33

control field pulses, which are calibrated by performing a simple nutation experiment on each of the corresponding transitions. Due to the complexity of the pulse sequence required for the experiment with the state $|D_{1,1}\rangle$, the results does not match the simulation well.

A maximum of the visibility occurs at $b/a = 1$, which implies that the dark state $|D_{1,1}\rangle$ has a maximum transparency value through the EIT evolution $U_{EIT,a,b}$, which is what we expect from our theoretical calculations in section 3.4.3.

In the next section, we carry out the same experiment with the state $|1\rangle$. Because we can use simpler pulse sequence for the experiments with the state $|1\rangle$, we expect the fidelity to be higher and the simulation matches the data better.

4.5   Visibility in the strong control field limit

Ramsey interferometry with the state $|1\rangle$, which is the dark state in the strong control field limit, and the state $|R\rangle$ is carried out (see section 3.4.2). The probe field strength a is set to a power that corresponds to $3\pi/2$ pulses, and the control field strength is varied from a to $7a$ at the given probe field strength. A $[\pi/2]_x$ pulse followed by a $\hat{z}$-rotation at the $|R\rangle \rightarrow |1\rangle$ transition frequency is used for the Hadamard gate. Then a $\hat{z}$-rotation at the same frequency is applied to add an overall phase θ to the dark state. The EIT Hamiltonian is applied at the given probe field and control field strengths. Finally, the Hadamard gate is again applied. The detailed pulse sequence is given in Appendix D.

We measure the observable $|R\rangle\langle 1|$ by applying a $[\pi/2]_x$ pulse at the $|R\rangle \rightarrow |1\rangle$ transition frequency. Visibility of this single quantum coherence is plotted in Fig. 4-4. The solid line is the ideal theory (see Eq. (3.24)), the dotted line is the simulation and the error bars are the experimental results. The experimental errors are obtained by repeating the experiment five times and taking the random errors. We believe that the sources of the errors are the noise in the FID signal and the temperature fluctuations in the experimental setup. As in section 4.4, the simulation includes the decoherence effects and the imperfections of the probe and control field pulses (see Appendix B for the code). The duration of the experiments is about $8.8ms$. The RF inhomogenity of the NMR probe is also taken into account and is measured by comparing the pulse sequence with a single readout. The results matches the simulation well.

The visibility increases as b/a gets larger. This implies that the system approaches
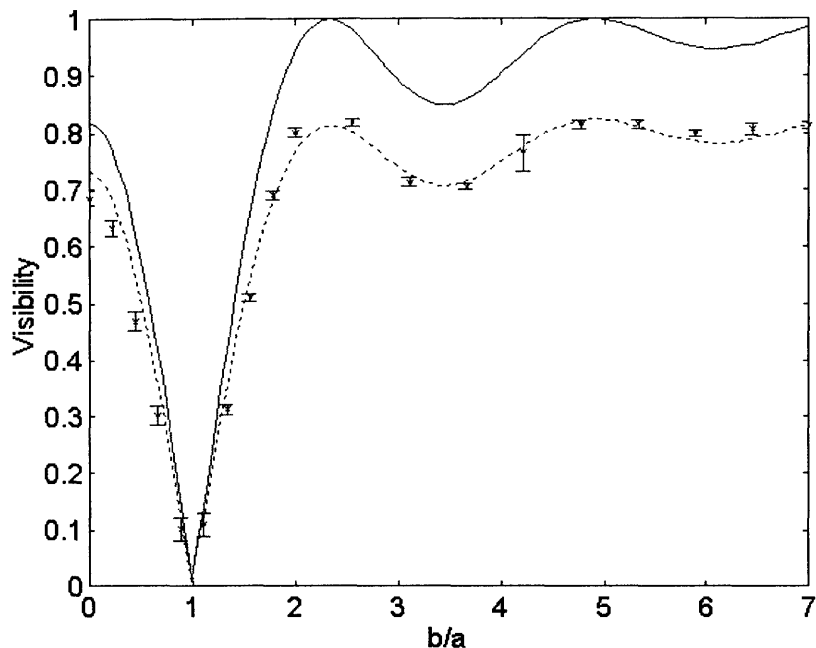
Figure 4-4: Visibility versus b/a when the the probe field strength corresponds to $3\pi/2$ pulses. The solid line is the ideal theory, the dotted line is the simulation and the error bars are the experimental results. The results falls below the ideal theory due to the decoherence effects and the RF inhomogenity of the NMR probe.

the dark state $|1\rangle$ with increasing b/a and that the state $|1\rangle$ has a maximum transparency value through the EIT evolution $U_{EIT,a,b}$ when $b/a \to \infty$, which is what we expect from our theoretical calculations in section 3.4.3. However, due to the limitations of the pulse power we can get while keeping the pulses selective enough, we are only able to show that the visibility slowly increases with b/a. The off-resonance excitations start to affect the experiments when the control field power corresponds to 11π pulses and change the results more than 10 percent from the expected results when the control field power corresponds to 15π pulses. These power corresponds to power settings of about 34dB and 37.5dB in the spectrometer setup, respectively.

The maximum visibility is about 82 percent. For improved visibility, we first need to eliminate the effects from the RF inhomogenity. This can be done by using a better NMR probe or using more complex composite pulses designed for this. However, there is a limit on the homogenity of a NMR probe. Using complex composite pulses may reduce the RF inhomogenity effect but, at the same time, will make it hard for us to model the system accurately. We can reduce the decoherence effects by using samples with longer

decoherence times or by reducing the pulse lengthes, which requires samples with larger splittings between the transition frequencies to keep the pulses selective enough. To perform the experiments at higher values of b/a, we need higher pulse power or longer pulse length. Again, higher pulse power requires larger splitting between the transition frequencies to keep the pulses selective enough. We can see the trade-off between the fidelity and the signal power.

Chapter 5

Conclusion

We have shown that quantum phenomenon in atomic systems such as the EIT effect can be realized in nuclear spin systems. We started by introducing a higher-order spin system that is equivalent to a Λ-like atomic system and showing how a higher-order spin system can be used to effciently simulate the EIT effect by NMR techniques. We presented two ways of verifying the transparency behavior of spin systems: the first one is observing the NMR signal corresponding to observables of the density matrix of the system and the second is measuring the visibility of the dark state after the EIT evolution through Ramsey interferometry. We provided experimental evidences of the transparency using these methods and also explained the discrepancy between the experimental results and the theory through the simulations. Finally, we have shown that the quantum phase of the dark state remains unchanged through Ramsey interferometry.

We believe that this thesis work is not merely a investigation of the EIT effect but a first step toward studying various quantum optical phenomena in nuclear spin systems.

Appendix A

Simulation for Bloch-Siegert Shifts

This appendix is the simulation code for Bloch-Siegert shifts for a spin-3/2 system [SVC00].

```
% File: bsshift.m
% Date: 24-May-02
% Modified: Matthias Steffen <msteffen@snowmass.stanford.edu
%
% calculates phase accumulation due to transient Bloch-Siegert shifts for
% the spin-3/2 subsystem of a spin-7/2 system.
% syntax:
% OP=bsshift(maxamp1,maxamp2,pulse_shape,pulse_width,offset,inphase)
%
% maxamp1 : pulse on 3rd line (1st for spin-3/2 subsystem)
% maxamp2 : pulse on 4th line (2nd for spin-3/2 subsystem)
% maxamp: 2 for pi pulse
%          1 for pi/2 pulse
% pulse_shape: the pulse shape file name. 'gauss.RF' for example
% pulse_width: the pulse width in microseconds
% offset: frequency separation between each of the transition frequency
function OP=bsshift(maxamp1,maxamp2,pulse_shape,pulse_width,offset,inphase)
%%%%%%%%%%%%%%%%%%%%%%%%%%%%%%%%%%%%%%%%%%%%%%%%%%%%%%%%%%%%%%
% Pauli sig_x and sig_y operators for each of the transitions %
%%%%%%%%%%%%%%%%%%%%%%%%%%%%%%%%%%%%%%%%%%%%%%%%%%%%%%%%%%%%%%
```

```matlab
global H1 H2 H3 H4 H5 H6 H7
global H1i H2i H3i H4i H5i H6i H7i
%%%%%%%%%%%%%%%%%%%%%%%%%%%%%%%
% read in original pulse shape %
%%%%%%%%%%%%%%%%%%%%%%%%%%%%%%%
library = 'Library directory name for pulse shape files';
dir=sprintf(['%s\\%s'],library, pulse_shape);
input=fopen(dir,'r');
in=1; time(1)=0; line=fgets(input);
while (line(1)=='#'),
 line=fgets(input);
end
while (line>0),
 line1=str2num(line);
 slicephase1(in)=line1(1)+inphase;
 sliceamp1(in)=line1(2);
 slicelength1(in)=line1(3);
 line=fgets(input);
 in=in+1;
end
fclose('all');


numslices=length(sliceamp1);
sliceamp2=sliceamp1;
slicelength2=slicelength1;


%%%%%%%%%%%%%%%%%%%%%%%%%%%%%%%%%%%%%%%%%%%%%%%%%%%%%%%%%%%%%%%%%%%
% set phase ramp 2 to excite at freq=offset (no BS correction yet) %
%%%%%%%%%%%%%%%%%%%%%%%%%%%%%%%%%%%%%%%%%%%%%%%%%%%%%%%%%%%%%%%%%%%


slicephase2=slicephase1;
if offset~=0
```

```
final_phase2=pulse_width*1e-6*(-offset)*360;
phasestep2=final_phase2/numslices;
slicephase2= slicephase2
            + [phasestep2/2:phasestep2:final_phase2-phasestep2/2];
slicephase2=mod(slicephase2,360);
end


slicephase3=slicephase1;
if offset~=0
final_phase3=pulse_width*1e-6*(-offset*2)*360;
phasestep3=final_phase3/numslices;
slicephase3= slicephase3
            + [phasestep3/2:phasestep3:final_phase3-phasestep3/2];
slicephase3=mod(slicephase3,360);
end


slicephase4=slicephase1;
if offset~=0
final_phase4=pulse_width*1e-6*(-offset*3)*360;
phasestep4=final_phase4/numslices;
slicephase4= slicephase4
            + [phasestep4/2:phasestep4:final_phase4-phasestep4/2];
slicephase4=mod(slicephase4,360);
end


slicephase5=slicephase1;
if offset~=0
final_phase5=pulse_width*1e-6*(-offset*4)*360;
phasestep5=final_phase5/numslices;
slicephase5= slicephase5
            + [phasestep5/2:phasestep5:final_phase5-phasestep5/2];
slicephase5=mod(slicephase5,360);
```

```
end


%%%%%%%%%%%%%%%%%%%%%%
% renormalize variables %
%%%%%%%%%%%%%%%%%%%%%%


slicephase1=slicephase1*pi/180;    % convert to radians

slicephase2=slicephase2*pi/180;    % convert to radians

slicephase3=slicephase3*pi/180;    % convert to radians

slicephase4=slicephase4*pi/180;    % convert to radians

slicephase5=slicephase5*pi/180;    % convert to radians

sliceamp1=sliceamp1/1023;          % renormalize such that max value is 1

sliceamp2=sliceamp2/1023;          % renormalize such that max value is 1

slicelength1=slicelength1/sum(slicelength1)*10^-6*pulse_width;

slicelength2=slicelength2/sum(slicelength2)*10^-6*pulse_width;
                              % convert to seconds
maxamp1=0.25*maxamp1
        /abs((sum(sliceamp1.*exp(i*slicephase1).*slicelength1)));
maxamp2=0.25*maxamp2
        /abs((sum(sliceamp1.*exp(i*slicephase1).*slicelength1)));


%%%%%%%%%%%%%%%%%%%%%%%%%%%%%%
% calculate phase accumulation  %
%%%%%%%%%%%%%%%%%%%%%%%%%%%%%%
% start from an identity operator
operator=eye(8);


% for each time slice, calculate the phase accumulation due to the pulses:
% maxamp1 : pulse on 3rd line (1st for spin-3/2 subsystem)
% maxamp2 : pulse on 4th line (2nd for spin-3/2 subsystem)
for index = 1:numslices
H_RF1=sliceamp2(index)*maxamp1*2*pi*
```

```
(cos(slicephase3(index))*H1 - sin(slicephase3(index))*H1i)/2;

H_RF2=sliceamp2(index)*maxamp1*2*pi*

(cos(slicephase2(index))*H2 - sin(slicephase2(index))*H2i)/2;

H_RF3=sliceamp2(index)*maxamp1*2*pi*

(cos(slicephase1(index))*H3 - sin(slicephase1(index))*H3i)/2;

H_RF4=sliceamp2(index)*maxamp1*2*pi*

(cos(slicephase2(index))*H4 + sin(slicephase2(index))*H4i)/2;

H_RF5=sliceamp2(index)*maxamp1*2*pi*

(cos(slicephase3(index))*H5 + sin(slicephase3(index))*H5i)/2;

H_RF6=sliceamp2(index)*maxamp1*2*pi*

(cos(slicephase4(index))*H6 + sin(slicephase4(index))*H6i)/2;

H_RF7=sliceamp2(index)*maxamp1*2*pi*

(cos(slicephase5(index))*H7 + sin(slicephase5(index))*H7i)/2;

H_RF8=sliceamp2(index)*maxamp2*2*pi*

(cos(slicephase4(index))*H1 - sin(slicephase4(index))*H1i)/2;

H_RF9=sliceamp2(index)*maxamp2*2*pi*

(cos(slicephase3(index))*H2 - sin(slicephase3(index))*H2i)/2;

H_RF10=sliceamp2(index)*maxamp2*2*pi*

(cos(slicephase2(index))*H3 - sin(slicephase2(index))*H3i)/2;

H_RF11=sliceamp2(index)*maxamp2*2*pi*

(cos(slicephase1(index))*H4 - sin(slicephase1(index))*H4i)/2;

H_RF12=sliceamp2(index)*maxamp2*2*pi*

(cos(slicephase2(index))*H5 + sin(slicephase2(index))*H5i)/2;

H_RF13=sliceamp2(index)*maxamp2*2*pi*

(cos(slicephase3(index))*H6 + sin(slicephase3(index))*H6i)/2;

H_RF14=sliceamp2(index)*maxamp2*2*pi*

(cos(slicephase4(index))*H7 + sin(slicephase4(index))*H7i)/2;


operator = expm ( -i * (H_RF1 + H_RF2 + H_RF3 + H_RF4 + H_RF5 + H_RF6 +
           H_RF7 + H_RF8 + H_RF9 + H_RF10+ H_RF11 + H_RF12 + H_RF12 +
           H_RF13 + H_RF14) * slicelength1(index) ) * operator;
```

```
cumul_phase(index)=2*phase(operator(1,1)); % is in radians
end;


% phase ramp spin 1 for advanced Bloch-Siegert correction
slicephase1 = slicephase1 + [0 mod(cumul_phase(1:numslices-1),2*pi)];


% phase ramp spin 2 for advanced Bloch-Siegert correction
slicephase2 = slicephase2 - [0 mod(cumul_phase(1:numslices-1),2*pi)];


%%%%%%%%%%%%%%%%%%%%%%%%%%%%%%%%%%%%%%%%%%%%%%%%%%%%%%
% extracts the operator for the spin-3/2 subsystem %
%%%%%%%%%%%%%%%%%%%%%%%%%%%%%%%%%%%%%%%%%%%%%%%%%%%%%%


OP1(1,1) = operator(3,3);
OP1(1,2) = operator(3,4);
OP1(1,3) = operator(3,5);
OP1(1,4) = operator(3,6);


OP1(2,1) = operator(4,3);
OP1(2,2) = operator(4,4);
OP1(2,3) = operator(4,5);
OP1(2,4) = operator(4,6);


OP1(3,1) = operator(5,3);
OP1(3,2) = operator(5,4);
OP1(3,3) = operator(5,5);
OP1(3,4) = operator(5,6);


OP1(4,1) = operator(6,3);
OP1(4,2) = operator(6,4);
OP1(4,3) = operator(6,5);
OP1(4,4) = operator(6,6);
```

```
OP=OP1;
```

Appendix B

Simulation for Ramsey interferometry with the state $|1\rangle$

This appendix includes the matlab codes for plotting the simulated results for Ramsey interferometry with the state $|1\rangle$.

```matlab
%%%%%%%%%%%%%%%%%%%%%%%%%%%%%%%%%%%%%%%%%%%%%%%%%%%%%%%%%%%%%%%%%%%%%%%%%%%%%
% plot the simulated results for the visibility with the state |1>
function anaV
% load the environment for some functions we use
quadmat;

% parameters

% probe field strength (in units of pi/2 pulses)
alen=1;  % use one probe field strength
as(1)=3; % 3 pi/2

% b/a values
bathy=linspace(0, 7);

% run simulations
for n=1:alen;
```

```matlab
    Vthy(n,:) = eitsimulationbgta(acalib(as(n)),bcalib(bathy*as(n)));
end;

% plot the results
plot(bathy, Vthy(1,:), 'b--');
axis([0 7 0 1]);
fontsize=16;
xlabel('b/a','FontSize',fontsize);
ylabel('Visibility','FontSize',fontsize);
set(gca,'FontSize', fontsize);


%%%%%%%%%%%%%%%%%%%%%%%%%%%%%%%%%%%%%%%%%%%%%%%%%%%%%%%%%%%%%%%%%%%%%%%%%%%%%
% quadmat.m
% defines Hamiltonians for the spin 7/2 system
% sig_x operators
global H1 H2 H3 H4 H5 H6 H7
% sig_y operators
global H1i H2i H3i H4i H5i H6i H7i
% thermal population
global rit

rit=diag([0 1 2 3 4 5 6 7]);

H1=[0 1 0 0 0 0 0 0; 1 0 0 0 0 0 0 0; 0 0 0 0 0 0 0 0; 0 0 0 0 0 0 0 0;
    0 0 0 0 0 0 0 0; 0 0 0 0 0 0 0 0; 0 0 0 0 0 0 0 0; 0 0 0 0 0 0 0 0;];
H1i=[0 -i 0 0 0 0 0 0; i 0 0 0 0 0 0 0; 0 0 0 0 0 0 0 0; 0 0 0 0 0 0 0 0;
    0 0 0 0 0 0 0 0; 0 0 0 0 0 0 0 0; 0 0 0 0 0 0 0 0; 0 0 0 0 0 0 0 0;];
H2=[0 0 0 0 0 0 0 0; 0 0 1 0 0 0 0 0; 0 1 0 0 0 0 0 0; 0 0 0 0 0 0 0 0;
    0 0 0 0 0 0 0 0; 0 0 0 0 0 0 0 0; 0 0 0 0 0 0 0 0; 0 0 0 0 0 0 0 0;];
H2i=[0 0 0 0 0 0 0 0; 0 0 -i 0 0 0 0 0; 0 i 0 0 0 0 0 0; 0 0 0 0 0 0 0 0;
    0 0 0 0 0 0 0 0; 0 0 0 0 0 0 0 0; 0 0 0 0 0 0 0 0; 0 0 0 0 0 0 0 0;];
H3=[0 0 0 0 0 0 0 0; 0 0 0 0 0 0 0 0; 0 0 0 1 0 0 0 0; 0 0 1 0 0 0 0 0;
```

```matlab
   0 0 0 0 0 0 0; 0 0 0 0 0 0 0; 0 0 0 0 0 0 0; 0 0 0 0 0 0 0;];
H3i=[0 0 0 0 0 0 0; 0 0 0 0 0 0 0; 0 0 0 -i 0 0 0; 0 0 i 0 0 0 0;
   0 0 0 0 0 0 0; 0 0 0 0 0 0 0; 0 0 0 0 0 0 0; 0 0 0 0 0 0 0;];
H4=[0 0 0 0 0 0 0; 0 0 0 0 0 0 0; 0 0 0 0 0 0 0; 0 0 0 0 1 0 0 0;
   0 0 0 1 0 0 0 0; 0 0 0 0 0 0 0; 0 0 0 0 0 0 0; 0 0 0 0 0 0 0;];
H4i=[0 0 0 0 0 0 0; 0 0 0 0 0 0 0; 0 0 0 0 0 0 0; 0 0 0 0 -i 0 0 0;
   0 0 0 i 0 0 0 0; 0 0 0 0 0 0 0; 0 0 0 0 0 0 0; 0 0 0 0 0 0 0;];
H5=[0 0 0 0 0 0 0; 0 0 0 0 0 0 0; 0 0 0 0 0 0 0; 0 0 0 0 0 0 0;
   0 0 0 0 0 1 0 0; 0 0 0 0 1 0 0 0; 0 0 0 0 0 0 0; 0 0 0 0 0 0 0;];
H5i=[0 0 0 0 0 0 0; 0 0 0 0 0 0 0; 0 0 0 0 0 0 0; 0 0 0 0 0 0 0;
   0 0 0 0 0 -i 0 0; 0 0 0 0 i 0 0 0; 0 0 0 0 0 0 0; 0 0 0 0 0 0 0;];
H6=[0 0 0 0 0 0 0; 0 0 0 0 0 0 0; 0 0 0 0 0 0 0; 0 0 0 0 0 0 0;
   0 0 0 0 0 0 0; 0 0 0 0 0 0 1 0; 0 0 0 0 0 1 0 0; 0 0 0 0 0 0 0;];
H6i=[0 0 0 0 0 0 0; 0 0 0 0 0 0 0; 0 0 0 0 0 0 0; 0 0 0 0 0 0 0;
   0 0 0 0 0 0 0; 0 0 0 0 0 0 -i 0; 0 0 0 0 0 i 0 0; 0 0 0 0 0 0 0;];
H7=[0 0 0 0 0 0 0; 0 0 0 0 0 0 0; 0 0 0 0 0 0 0; 0 0 0 0 0 0 0;
   0 0 0 0 0 0 0; 0 0 0 0 0 0 0; 0 0 0 0 0 0 0 1; 0 0 0 0 0 0 1 0;];
H7i=[0 0 0 0 0 0 0; 0 0 0 0 0 0 0; 0 0 0 0 0 0 0; 0 0 0 0 0 0 0;
   0 0 0 0 0 0 0; 0 0 0 0 0 0 0; 0 0 0 0 0 0 0 -i; 0 0 0 0 0 0 i 0;];


%%%%%%%%%%%%%%%%%%%%%%%%%%%%%%%%%%%%%%%%%%%%%%%%%%%%%%%%%%%%%%%%%%%%%%%%
% calculate the visibility of the state |1>
% at the probe field stength a and the control field
% strengths given in bArray.
function vis = eitsimulationbgta(a,bArray);
% the angle theta required for calculating visibility
thetaArray=[0 2];
for bIndex=1:length(bArray);
   % run the simulation with parameters
   b=bArray(bIndex);
   for thetaIndex=1:length(thetaArray)
      theta=thetaArray(thetaIndex);
```

```
        p(thetaIndex)=eit_bgta(a,b,theta);
    end;
    % calculate the visibility
        Imax(bIndex)=max(p);
        Imin(bIndex)=min(p);
    vis(bIndex)=(Imax(bIndex)-Imin(bIndex))/(Imax(bIndex)+Imin(bIndex));
end;


%%%%%%%%%%%%%%%%%%%%%%%%%%%%%%%%%%%%%%%%%%%%%%%%%%%%%%%%%%%%%%%%%%%%%%
% Simulate the readout peak for
% the Ramsey interferometry
% with the probe field strength a
% and the control field strength b.
% The phase of the dark state is theta.
function p=eit_beqa(a,b,theta)
% the Hadamard gate
H=Zq(3,2)*Yq(3,1);
% the phase for the dark state
PHT=Zq(3,theta);
% the EIT Hamiltonian
Heit=[0 b 0 0;b 0 a 0;0 a 0 0 ;0 0 0 0;]/2*pi/2;


% temporal labeling.
dens0(1,:,:)=diag([4 3 2 1]/10);
dens0(2,:,:)=diag([2 3 4 1]/10);
% Hamiltonian for y-rotation
sig_y3 = [ 0 0 0 0; 0 0 0 0; 0 0 0 -i; 0 0 i 0];
% set where to apply the Lindblad relaxation
ideal=0; idealeit=1;
% the length of the pulses (ms)
TQ = .62;
% the length of the EIT evolution (ms)
```

```
Teit = 6;
% nomalization factor for the readout
p0= .5/10;
for labeling = 1:1
    % get initial density matrix
    dens=squeeze(dens0(labeling,:,:));
    % apply the Hadamard gate
    if ideal==1
        dens=Yq(3,1)*dens*Yq(3,1)';
    elseif ideal==0
        dens=relaxdens( dens, sig_y3*pi/2/2 /TQ, TQ);
    end;


    U =PHT*Zq(3,2); % finish the Hadamard and add phase to the dark state.
    dens=U*dens*U';


    % apply the EIT Hamiltonian
    if idealeit==0
        dens=expm(-i*Heit)*dens*expm(i*Heit);
    elseif idealeit==0
        dens=relaxdens( dens, Heit/Teit, Teit);
    end;


        % apply the Hadamard gate
    if ideal==1
        dens=Yq(3,1)*dens*Yq(3,1)';
    elseif ideal==0
        dens=relaxdens( dens, sig_y3*pi/2/2 /TQ, TQ);
    end;


        U =Zq(3,2);
        dens=U*dens*U';
```

```
        % apply the readout pulses
        dens3 = Xq(3,1)*dens*Xq(3,1)';


        p3(labeling)=imag(dens3(3,4));


        if theta==2
        % this is the factor due to the RF inhomogenity
      p3 = p3*.84;
    end;
end;
%readout of the peak
p3=mean(p3)/p0;
p=p3+1;
```

Appendix C

Lindblad equation for higher-order spin systems

```
% Relaxation model for higher-order spin systems using Lindblad equation
% Authors: Ben Recht, Murali Kota and Hyung-Bin Son
%
% rho - input density matrix
% H - Hamiltonian active during the relaxation process
% T - time upto which we wish to relax our system
% numpts - for accuracy

function rho = relaxdens(rho, H, T, numpts)

% Number of points defines the accurracy of the recursive
% algorithm for solving differential equation (in our case
% Schrodinger equation) using Euler's method

if ~exist('numpt')
   numpts=1000;
end;

% The step size of the time in solving the Schrodinger equation
```

```
% using Euler's method


deltat = T/numpts;

hbar=1;                 % as the theorists like it


% transitions are numbered lowest to highest.  the associated decay
% times are given by, times are in ms


T1_12=50;               % T1 relaxation time for transition 1

T1_23=100;              % T1 relaxation time for transition 2

T1_34=50;               % T1 relaxation time for transition 3


% The equilibrium density matrix
% Feed in a valid density matrix and set T big enough (about 5*100)
% to find the density matrix reaching equilibrium


rho_eq=diag([4 3 2 1]/10);


% Now we can create the generators of the Lindblad equation:
% the associated constants are as derived in chapter 4
g1=1/T1_12;

g2=1/T1_23;

g3=1/T1_34;


q1=rho_eq(1,1);

q2=rho_eq(2,2);

q3=rho_eq(3,3);

q4=rho_eq(4,4);


b1=g1*q2/q1;

b2=g2*q3/q2;

b3=g3*q4/q3;
```

```matlab
% and the corresponding Linblad operators in matrix from are given by
L0=zeros(4,4);
L0(1,2)=sqrt(g1);
L0(2,1)=sqrt(b1);
L0L0 = L0'*L0;


L1=zeros(4,4);
L1(2,3)=sqrt(g2);
L1(3,2)=sqrt(b2);
L1L1 = L1'*L1;


L2=zeros(4,4);
L2(3,4)=sqrt(g3);
L2(4,3)=sqrt(b3);
L2L2 = L2'*L2;


% Solving the Schrodinger equation using Euler's recursive
% iteration method
for k=1:numpts
    rho = rho + ( -i* (H*rho - rho*H) - 0.5*L0'*L0*rho - 0.5*rho*L0L0
        + L0*rho*L0' - 0.5*L1L1*rho - 0.5*rho*L1L1  + L1*rho*L1'
        - 0.5*L2L2*rho - 0.5*rho*L2L2 + L2*rho*L2') *deltat;
end
```

Appendix D

Pulse sequence for EIT in the strong control field limit

This appendix is the pulse sequence for the visibility and density matrix evolution in the strong control field limit (see section 4.2 and 4.4).

```
%   Author: M. Steffen <msteffen@snowmass.stanford.edu>
%           Hyungbin Son <being@mit.edu>
%
%   Pulse sequence for EIT experiment in the strong control field limit
%
%   XP, YP and ZP represent the pulse corresponding x,y and z-rotations
%   For example, XP(i, theta) is the x-rotation on the ith transition with
%       a power corresponding to (theta * pi/2) pulses.
%   First transition : |3> <-> |2>
%   Second transition : |2> <-> |1>
%   Third transtion : |1> <-> |R>

#include <standard.h>
#include "eitframe3.c"

mypulsesequence()
{
```

```
SetRFChanAttr(RF_Channel[1],SET_GATE_MODE,160,SET_XGMODE_VALUE,0,NULL);

SetRFChanAttr(RF_Channel[2],SET_GATE_MODE,160,SET_XGMODE_VALUE,0,NULL);

SetRFChanAttr(RF_Channel[3],SET_GATE_MODE,160,SET_XGMODE_VALUE,0,NULL);

SetRFChanAttr(RF_Channel[4],SET_GATE_MODE,160,SET_XGMODE_VALUE,0,NULL);
updt_interfiddelay(1.0*INOVA_STD_APBUS_DELAY);


status(A);              % Delay between experiments for thermalization
  delay(d1);


status(B);              % Temporal labeling


 if(ptype==0) {}        % Thermal state


 if(ptype==1) {         % With populations of |1> and |3> interchanged,
   XP(1,2);XP(2,2);XP(1,2);% Used when running EIT for visibility
 }
 if(ptype==2) {         % With populations of |2> and |3> interchanged
   XP(1,2);             % Used when running EIT for density matrix evolution
 }


status(C);
 if (etype==00) {       % 1. If running EIT for visibility
                        % in the strong control field limit,
   YP(3,1); ZP(3,2);    % Hadamard in the |R> and |1> basis
   ZP(3, zangle);       % The z-rotation for the phase for Ramsey
   EIT(tangle, dangle);% 'tangle' specifies the control field strength and
                        % 'dangle' specifies the probe field strength
   YP(3,1); ZP(3,2);    % Hadamard in the |R> and |1> basis
   XP(final,1);         % 'final' specifies the transition to readout
 }


                        % 2. If running power calibration
```

58

```
if (etype==1) {XP(1,2);} % pi pulse calibration on transition 1

if (etype==2) {XP(2,2);} % pi pulse calibration on transition 2

if (etype==3) {XP(3,2);} % pi pulse calibration on transition 3



if (etype==21) {XP(3,1);}% 3. Four tests in RF inhomogenity

if (etype==22) {YP(3,1); YP(3,1); XP(3,1); }

if (etype==23) {YP(3,1); YP(3,1); ZP(3,2); XP(3,1); }

if (etype==24) {YP(3,1); ZP(3,2); YP(3,1); XP(3,1); }


if (etype==4) {          % 4. If running EIT for density matrix evolution
  EIT(tangle, dangle);}

}
```

Appendix E

Pulse sequence for EIT using coherent dark states

This appendix is the pulse sequence for creating coherent dark states and testing visibility using Ramsey interferometry.

```
%    Author: Murali Kota <muralik@media.mit.edu>
%            Matthias Steffen <msteffen@snowmass.stanford.edu>
%    Pulse sequence for creating coherent dark states and
%      testing visibility using Ramsey interferometry.
%
%    XP, YP and ZP represent the pulse corresponding x,y and z-rotations
%    For example, XP(i, theta) is the x-rotation on the ith transition with
%        a power corresponding to (theta * pi/2) pulses.
%    First transition : |R> <-> |1>
%    Second transition : |1> <-> |2>
%    Third transtion : |2> <-> |3>

#include <standard.h>
#include "csframeeit4.c"

mypulsesequence()
```

```
{
SetRFChanAttr(RF_Channel[1],SET_GATE_MODE,160,SET_XGMODE_VALUE,0,NULL);

SetRFChanAttr(RF_Channel[2],SET_GATE_MODE,160,SET_XGMODE_VALUE,0,NULL);

SetRFChanAttr(RF_Channel[3],SET_GATE_MODE,160,SET_XGMODE_VALUE,0,NULL);

SetRFChanAttr(RF_Channel[4],SET_GATE_MODE,160,SET_XGMODE_VALUE,0,NULL);

updt_interfiddelay(1.0*INOVA_STD_APBUS_DELAY);


status(A);              % Delay between experiments for thermalization
 delay(d1);


status(B);              % Temporal labeling
 if(ptype==0) {}        % Thermal state


 if(ptype==1) {         % With populations of |1> and |3> interchanged,
   XP(3,2);XP(2,2);XP(3,2);
 }


status(C);              % Superposition of |1> and |3>
 if (ctype==1){
   YP(1,1); XP(2,1); XP(3,2);% Creates a superposition |1> - |3>
   ZP(3,atype); ZP(1,atype);% The z-rotations for the phase for Ramsey
 }


status(D);
 if (ftype==0) {}
 if (ftype==1) {        % EIT starts here
   EIT(eittype);        % eittype specifies the power of the control field
   XP(3,2);             % This is Hadamard in |R> and |D> basis
   XP(2,1);
   YP(1,-1); ZP(3,2); ZP(2,4); ZP(1,2);
   XP(2,1);
   XP(3,2);
```

```
   ZP(1,3); ZP(2,2); ZP(3,1);

                         % Hadamard runs upto here, after quite some work
}
 if(etype==0){          % Readouts for density matrix reconstruction
 }
 if(etype==1){
   XP(1,1);}
 if(etype==2){
   XP(2,1);}
 if(etype==3){
   XP(3,1);}
 if(etype==4){
   XP(2,2);}
 if(etype==5){
   XP(3,2); YP(2,2);}
}
```

Bibliography

[Abr83]   A. Abragam. *Principles of Nuclear Magnetism.* Clarendon Press, Oxford, 1983.

[CFH97]   D. G. Cory, A. F. Fahmy, and T. F. Havel. Ensemble quantum computing by NMR spectroscopy. *Proc. Natl. Acad. Sci. USA*, **94**, 1634–1639, 1997.

[DLCZ01]   L. M. Duan, M. D. Lukin, J. I. Cirac, and P. Zoller. Long-distance quantum communication with atomic ensembles and linear optics. *Nature*, **414**, 413, 2001.

[Fun01]   B. Fung. The use of pseudopure states for nmr quantum computing. *Phys. Rev. A*, **63**, 022304, 2001.

[GC97]   N. Gershenfeld and I. L. Chuang. Bulk spin resonance quantum computation. *Science*, **275**, 350, 1997.

[Har97]   S. E. Harris. Electromagnetically induced transparency. *Phys. Today*, **50**, 36, 1997.

[HFK92]   S. E. Harris, J. E. Field, and A. Kasapi. Dispersive properties of electromagnetically induced transparency. *Phys. Rev. A*, **46**, R29, 1992.

[HH99]   S. E. Harris and L. V. Hau. Nonlinear optics at low light levels. *Phys. Rev. Lett.*, **82**, 4611 – 4614, 1999.

[HHDB99]   L. V. Hau, S. E. Harris, Z. Dutton, and C. H. Behroozi. Light speed reduction to 17 meters per second in an unltracold atomic gas. *Nature*, **397**, 594 – 598, 1999.

[KCL98]   E. Knill, I. Chuang, and R. Laflamme. Effective pure states for bulk quantum computation. *Phys. Rev. A*, **57**(5), 3348–3363, 1998. URL: http://link.aps.org/volpage?journal=PRAvolume=57id=3348

[KF00]   A. Khitrin and B.M. Fung. Nuclear magnetic resonance quantum logic gates using quadrupolar nuclei. *Journal of Chemical Physics*, **112**, 6963 – 6965, 2000.

[KSM$^+$02] K.V.R.M.Murali, N. Sinha, T.S. Mahesh, M. Levitt, K. Ramanathan, and A. Kumar. Quantum-information processing by nuclear magnetic resonance: Experimental implementation of half-adder and subtractor operations using an oriented spin-7/2 system. *Phys. Rev. A.*, **66**, 022313, 2002.

[LDBH01] C. Liu, Z. Dutton, C. H. Behroozi, and L. V. Hau. Observatino of coherent optical information storage in an atomic medium using halted light pulses. *Nature*, **409**, 490 – 493, 2001.

[LYF00]   M. D. Lukin, S. F. Yelin, and M. Fleischhauer. Entanglement of atomic ensembles by trapping correlated photon states. *Phys. Rev. Lett.*, **84**, 4232, 2000.

[Mur03]   K. V. R. M. Murali. An approach to bridging atom optics and bulk spin quantum computation. Master's thesis, Massachusetts Institute of Technology, 2003.

[Pan01]   T. Pang. Electromagnetically induced transparency. *Am. J. Phys.*, **69**, 604, 2001.

[PFWL01] D. F. Phillips, A. Fleischhauer, R. L. Walsworth, and M. D. Lukin. Storage of light in atomic vapor. *Phys. Rev. Lett.*, **86**, 783 – 786", 2001.

[Sli96]   Charles P. Slichter. *Principles of Magnetic Resonance*. Springer, Berlin, 1996.

[SMP88]   D. Suter, K. T. Mueller, and A. Pines. Study of the aharonov-anandan quantum phase by nmr interferometry. *Phys. Rev. Lett.*, **60**, 1218, 1988.

[SVC00]   M. Steffen, L.M.K. Vandersypen, and I.L. Chuang. Simultaneous soft pulses applied at nearby frequencies. *J. Magn. Reson.*, **146**, 369–374, 2000.

[VL98]   L. Viola and S. Lloyd. Dynamical suppression of decoherence in two-state quantum systems. *Phys. Rev. A*, **58**(4), 2733 – 2744, 1998.